Supplement

"Chromatin decondensation and nuclear softening accompany Nanog downregulation in embryonic stem cells"

by K. J. Chalut, *et al.*

In this work, we show that ES cells primed for differentiation are associated with a state with softer cell and nuclear mechanics caused by a globally decondensed state of chromatin.

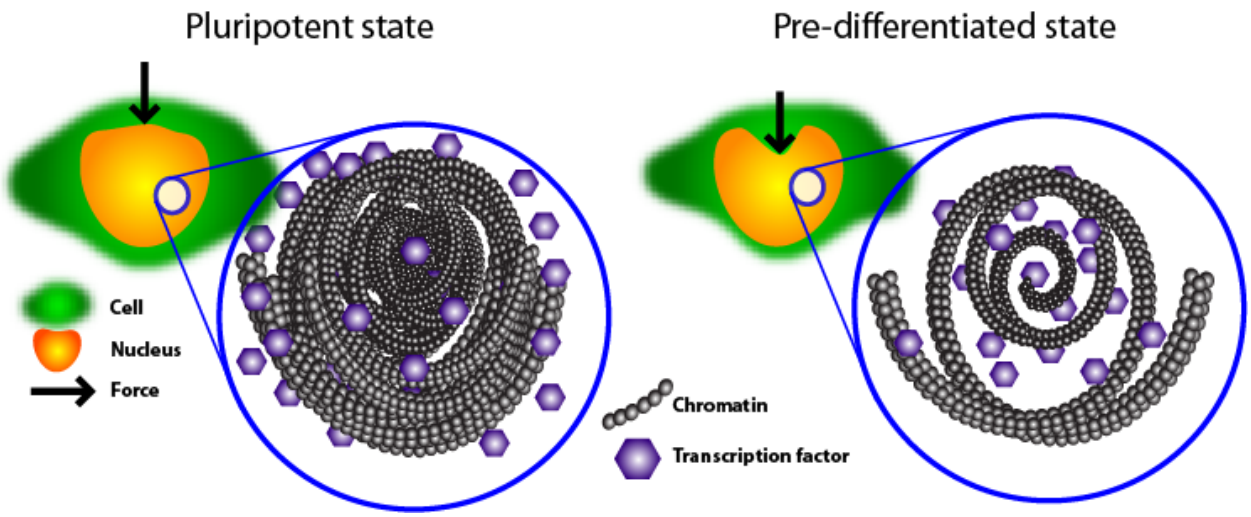

Supplemental Results

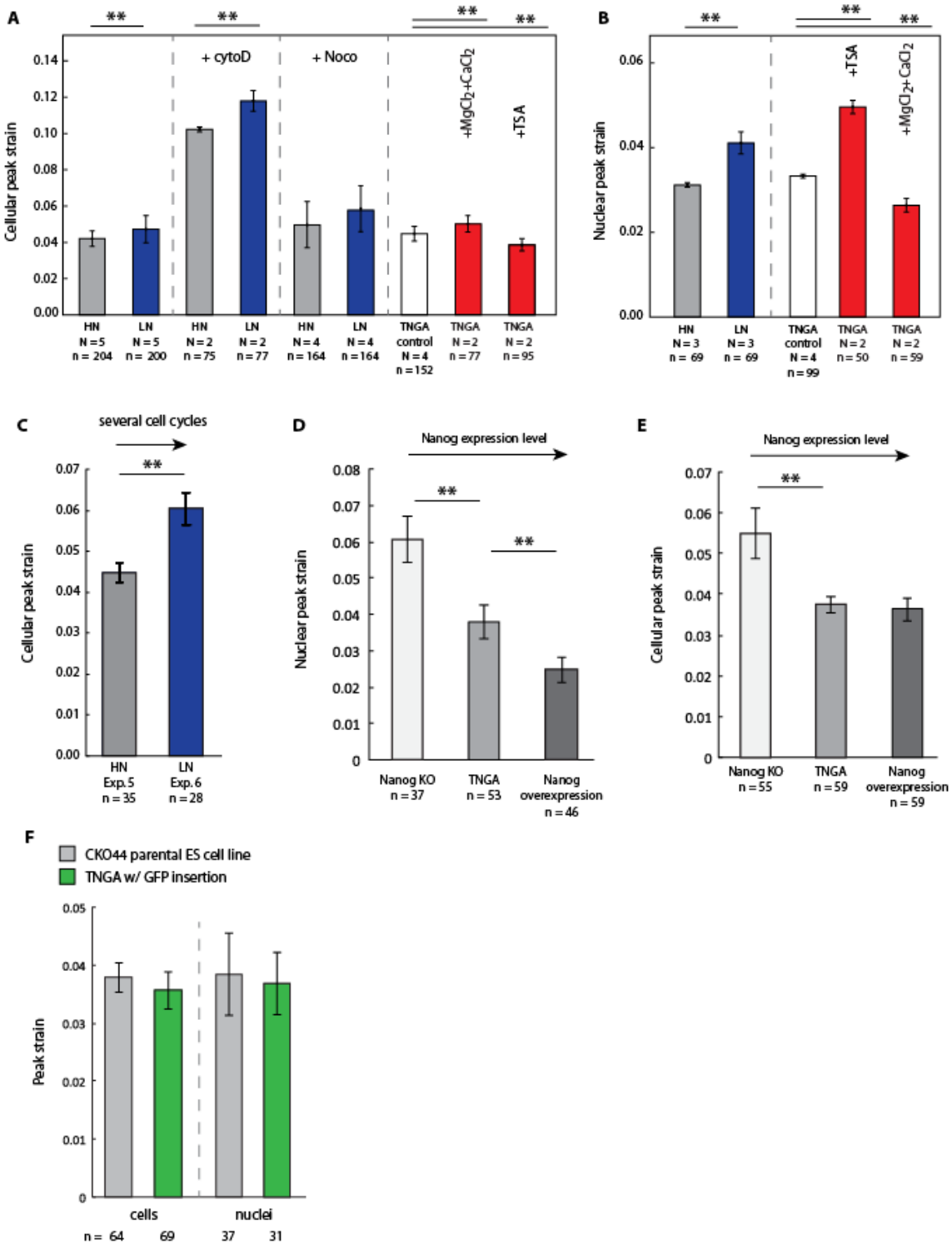

Fig. S1. Optical stretcher measurements show reproducible differences in cell and nuclear mechanics. The bars represent the replicate mean of each experiment while the error bar represents standard deviation of those means. N is the number of experiments and n is the total number of cells/nuclei measured for each condition. Results for whole cell strain (A) and nucleus strain (B) are

presented here. (C) HN cells were cultured for several passages (after experiment 5) and sorted into HN and LN cells after they recovered their original GFP-profile. LN cells obtained from these cells were more compliant in experiment 6 than HN cells in experiment 5. (D) Nuclear deformability decreases with expression levels of Nanog. Nuclear peak strain was compared between a Nanog Null knock-out cell line, TNGA cells and a Nanog overexpression cell line (RHN). (E) Nanog KO cells are more deformable than cells that express Nanog. These experiments correspond to the ones in (D) but whole cell deformability was measured. The correlation between nuclear and cellular deformability is not absolute, probably due to other, cytoplasmic factors. (F) We investigated the parent cell line for TNGAs to evaluate the effect of GFP insertion on mechanics. There is no significant difference in either cell or nuclear mechanics as an effect of GFP insertion.

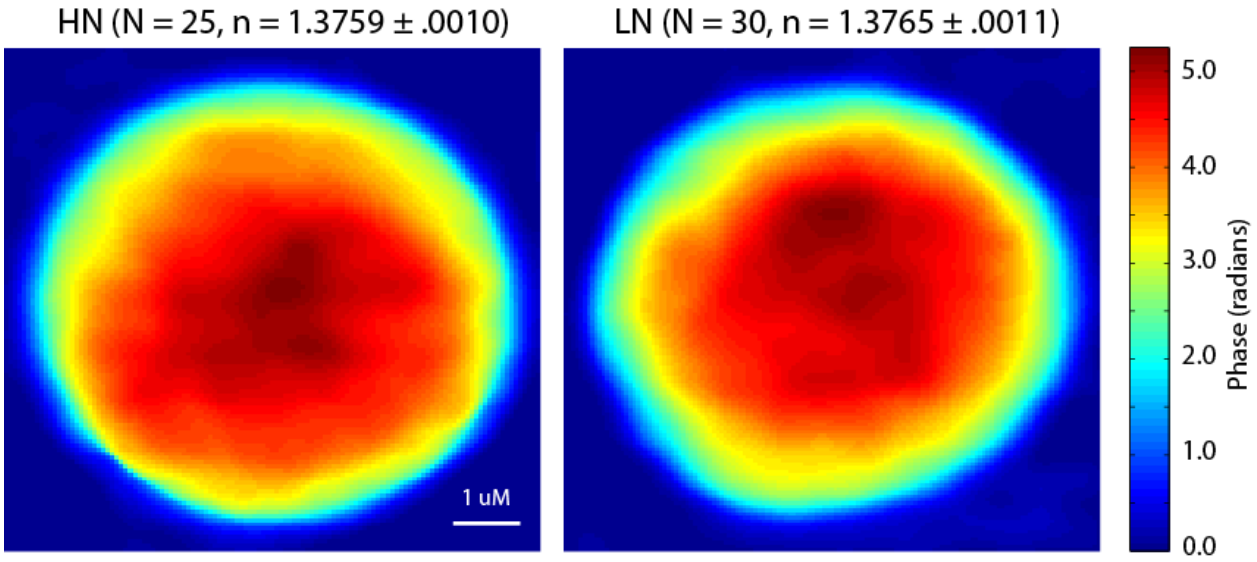

Fig. S2. DHM measurements show no difference in optical properties of HN and LN cells. Digital holographic microscopy (DHM) is a method for measuring quantitative phase variations in living cells. At left is a representative image of an HN cell, and at right is a representative image of an LN cell. We evaluated a population of each and found the average refractive index for each population (given in parentheses at top). There was no difference in refractive index between the two populations, and this information was used to find the compliance of the cells for Fig. 2 in the manuscript.

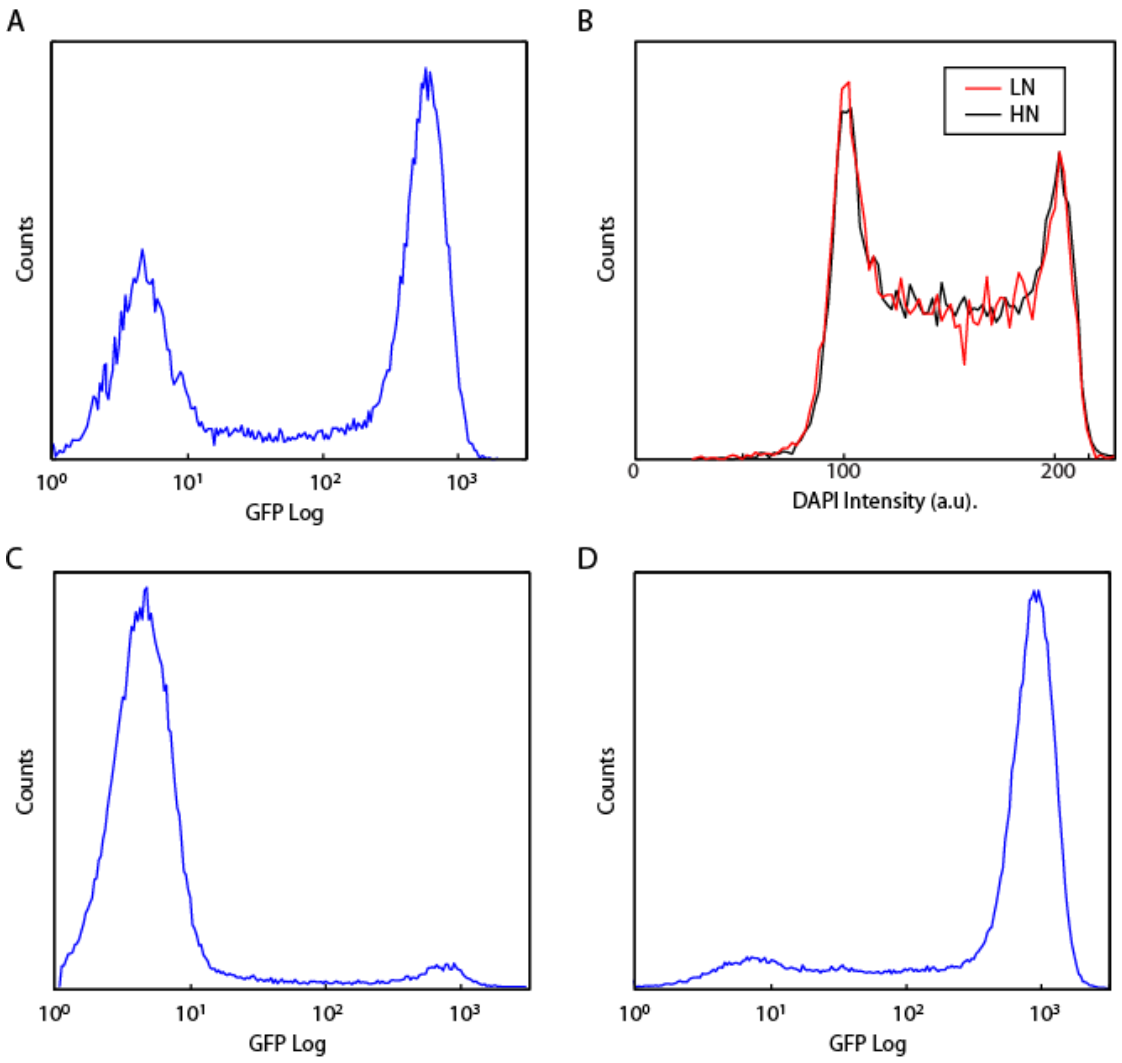

Fig. S3. **GFP profile and cell cycle distributions of TNGAs.** In (A), the unsorted GFP profile is shown for TNGAs as analyzed by flow cytometry. GFP is under control of the Nanog promoter. Note that approximately 30-35% of cells are GFP negative, indicating LN state, while over 50% of cells are GFP positive, indicating HN state. (B) The cell cycle distribution of HN and LN cells are nearly identical as shown by DAPI staining of TNGAs. After two days, there was negligible shift from LN to HN state and vice versa. Cells were sorted between GFP negative and GFP positive and measured 4 days later, at which point a shift from LN to HN (C) and vice versa (D) becomes apparent. Although the HN and LN state are fairly stable over time, the states are dynamic and transitions between them occur.

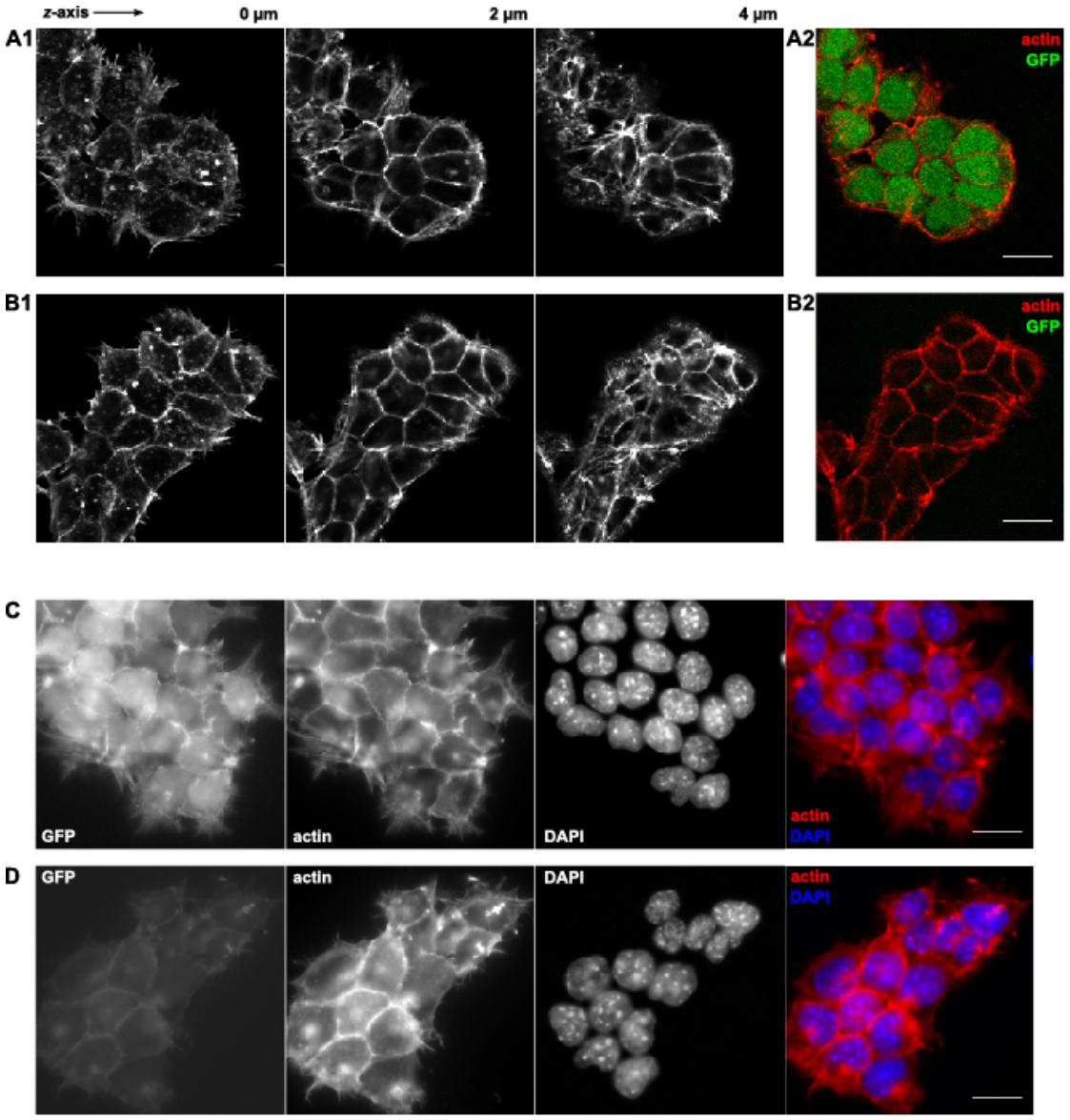

Fig. S4. No difference is observed in actin microfilament distributions between HN and LN cells. These observations are made with confocal (A,B) and epi-fluorescence (C,D) images of phalloidin-Alexa Fluor 546 dye and DAPI-stained TNGAs with GFP under control of Nanog promoter. (A1) and (B1) represent confocal stacks of actin stains. See Supplemental methods for staining protocols.

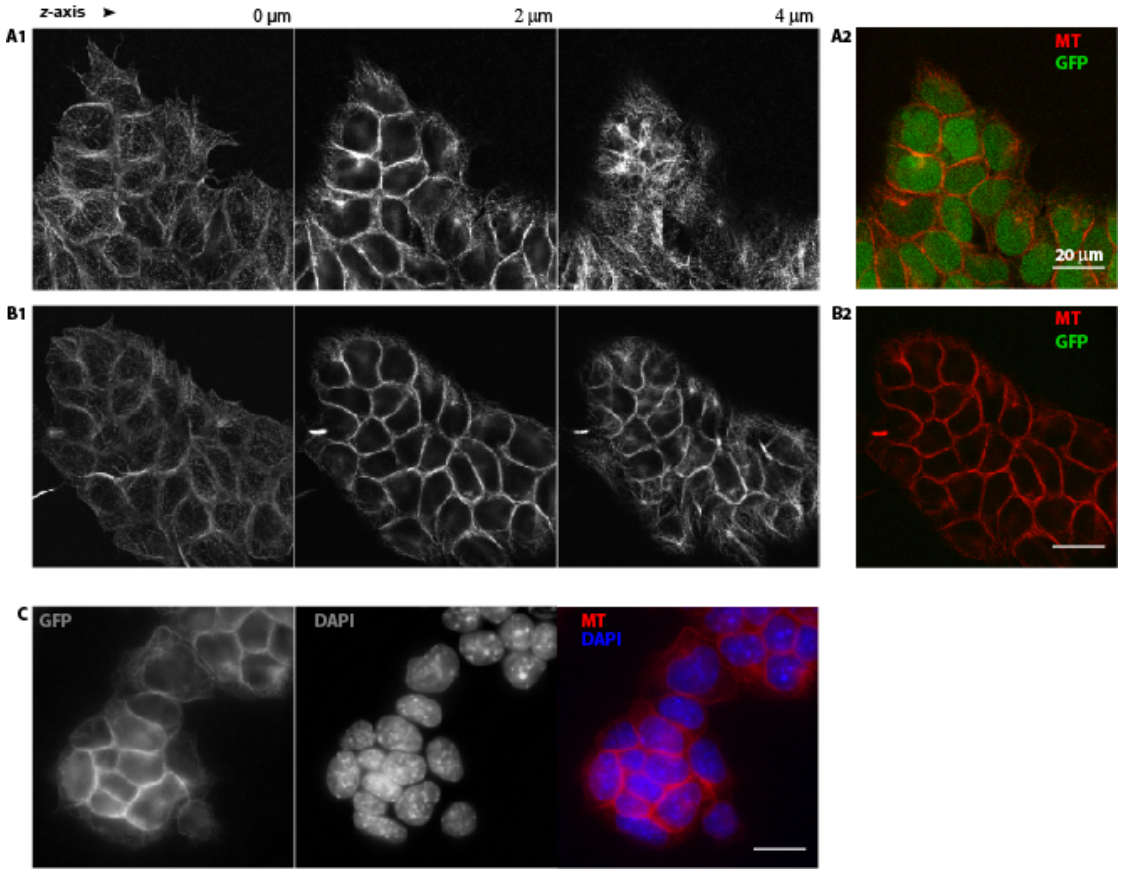

Fig. S5. No difference is observed in microtubule distributions between HN and LN cells. These observations are made with confocal (A,B) and epi-fluorescence (C) images of stained microtubules and nuclei of TNGAs, where GFP is under control of Nanog promoter. (A1) and (B1) represent confocal stacks of microtubules. For staining protocols see Supplemental Methods.

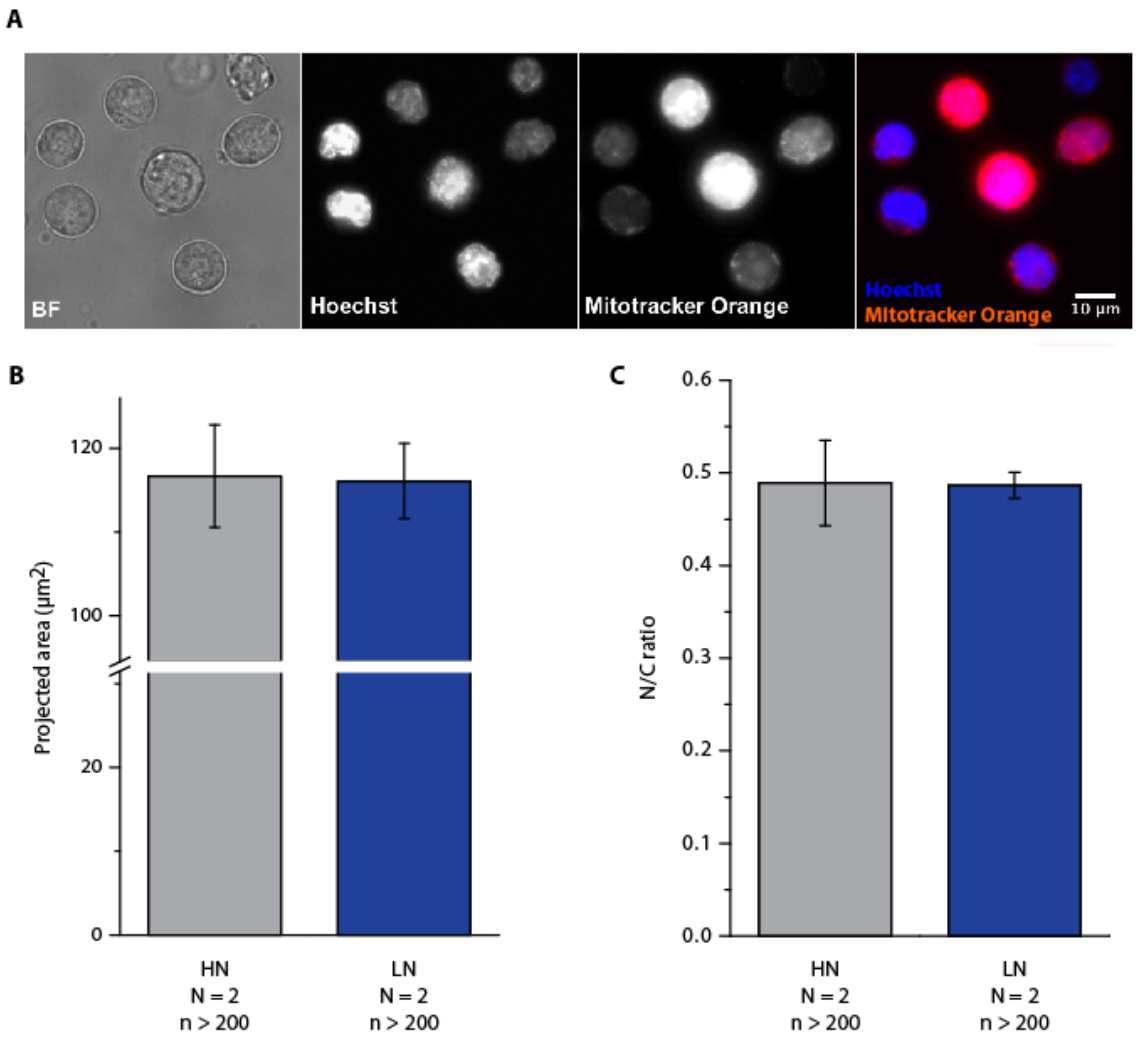

Fig. S6: There is no observed difference in morphology between HN and LN. (A) TNGAs were stained with Hoechst and Mitotracker Orange to distinguish between the nucleus and cytoplasm, and from this projected cell area (B) and nuclear to cytoplasmic ratio (C) were calculated.

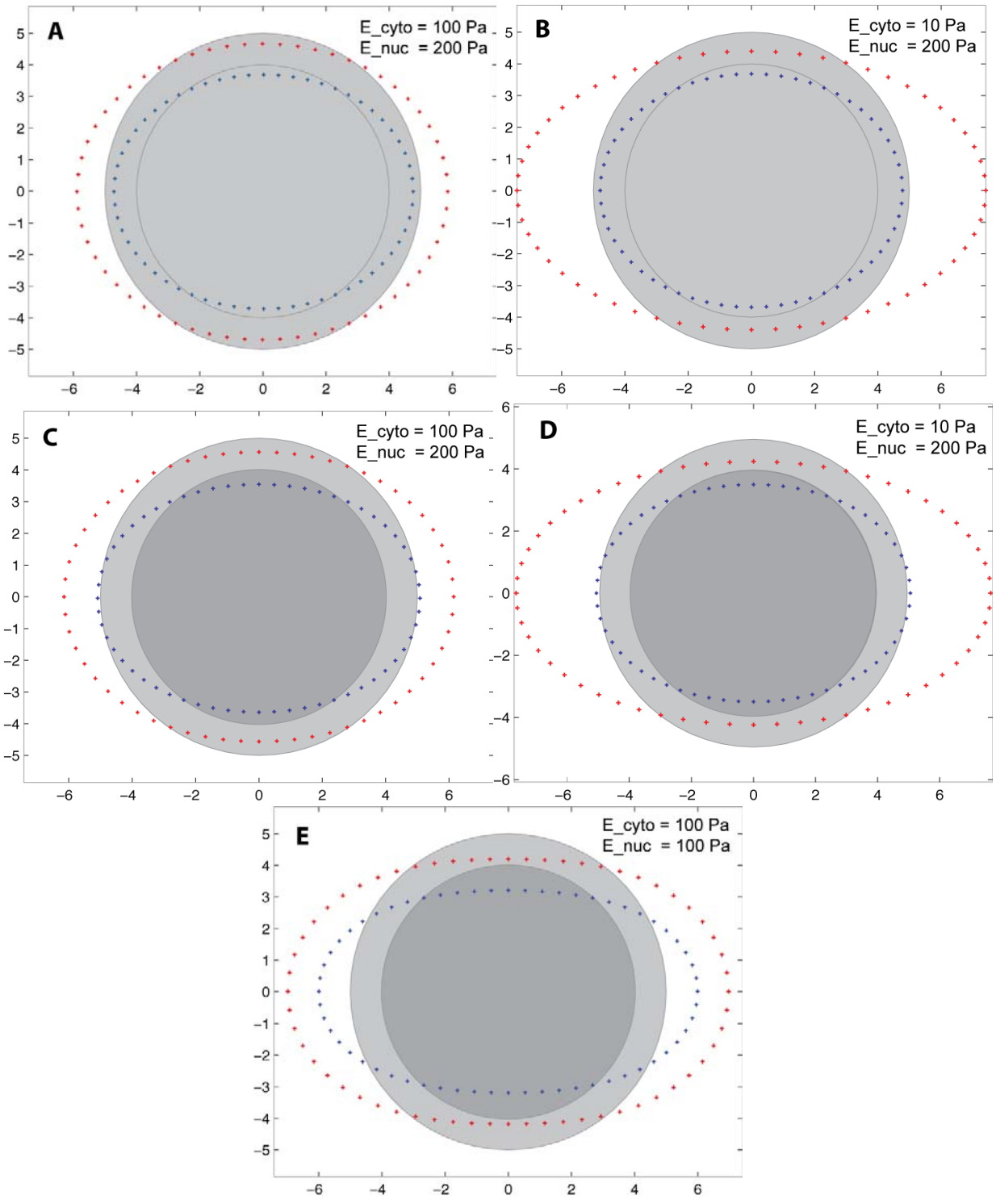

Fig. S7: Mechanical modelling of cell and nuclear deformation in an optical stretcher. To better illustrate the novel nuclear stretching technique, this series shows the results of continuum mechanical modelling of cell and nuclear deformation in the optical stretcher under various scenarios. Modelling was done according to that described in Ananthakrishnan, *J. Theo. Biol.*, 2006. In all cases there is an optically induced stress applied to the outer surface of the cell, which has a typical $\cos^2$-distribution (see Boyde et al., *Appl. Opt.*, 2012), and a peak stress of 50 Pa (chosen such that the resulting

deformations become obvious). The red dots signify the cellular deformation and the blue dots the nuclear deformation from the non-deformed spherical shapes. Grey scales indicate the refractive index. Respective stiffness of cytoplasm and nucleus is indicated in the panels. (A) Even when there is no optical stress on the nucleus, both cell and nucleus deform. (B) A reduction of the cytoplasmic stiffness leads to a significant increase in the cellular deformation but has very little consequence for the observed nuclear deformation. (C) Additional stress induced at the, now optically distinct, nucleus leads to a larger cellular and nuclear deformation. (D) However, a softening of the cytoplasm still has little impact on the resulting nuclear deformation (*cf.* C). These results demonstrate that cytoplasmic, incl. cytoskeletal, modifications (see also Fig. S8), even resulting in stiffness changes by an order of magnitude, with or without optical stress acting on the nucleus, impact nuclear deformations observed in the optical stretcher only very slightly. This should be compared to the effect of changes in the stiffness of the nucleus itself (E), where even the reduction by a factor of 2 leads to a significantly larger nuclear deformation by the same factor (*cf.* C). Overall, this modelling allows the conclusion that, in the absence of optical properties between LN and HN cells (see Fig. S2), the observed differences in nuclear deformation between LN and HN cells are not due to any changes of the cytoplasm between the two states, but have to come from mechanical differences of the nuclei themselves.

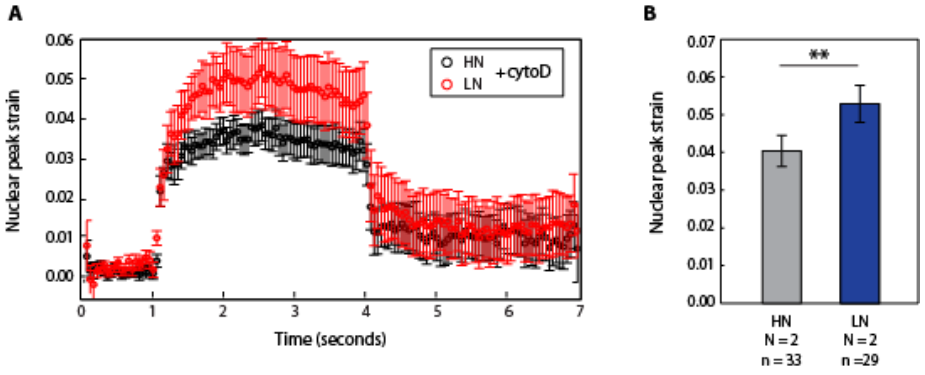

Fig. S8. Disrupting the cytoskeleton of TNGAs does not alter the relative differences in nuclear deformability. After treatment with CytoD, the nucleus of LN cells is significantly more deformable than HN cells as seen from differences in strain versus time (A) and nuclear peak strain (B). The fact that there is no relative difference between the peak strain here and when the cells are not treated with CytoD (see Fig. 2) indicates that the differences are not due to a pulling of the nucleus by the cytoskeleton.

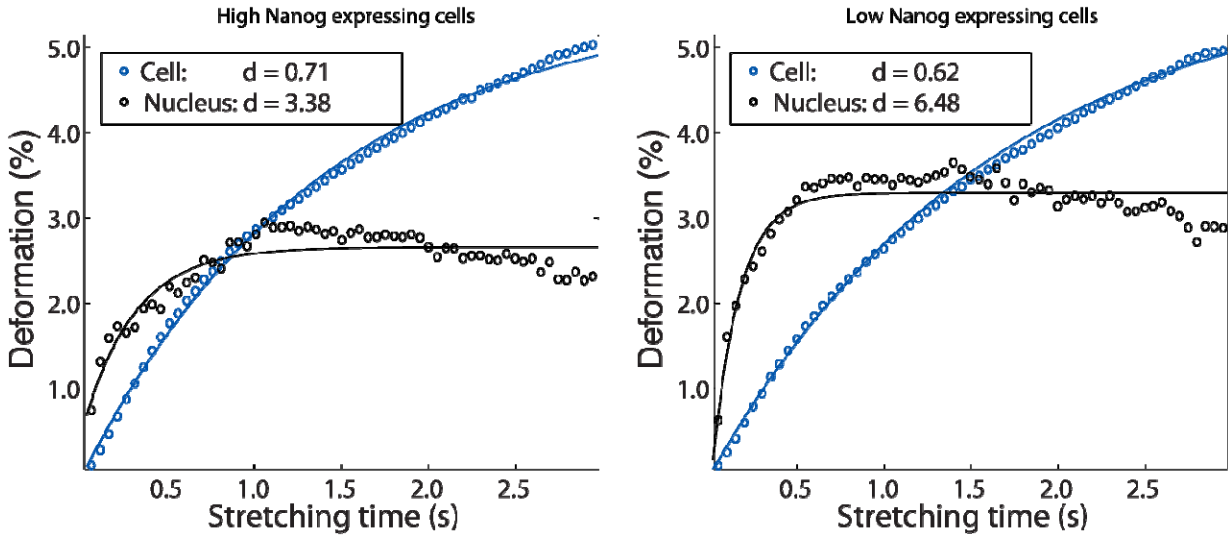

Fig. S9. The nucleus is more of an elastic solid than the cell. Using the standard liquid solid model of viscoelasticity (see reference (22) from main text), we can calculate a parameter *d*, from the nuclear and cell stretching data. *d* represents the ratio of elasticity to viscosity; from this we see that the nucleus is a more elastic solid than the cell.

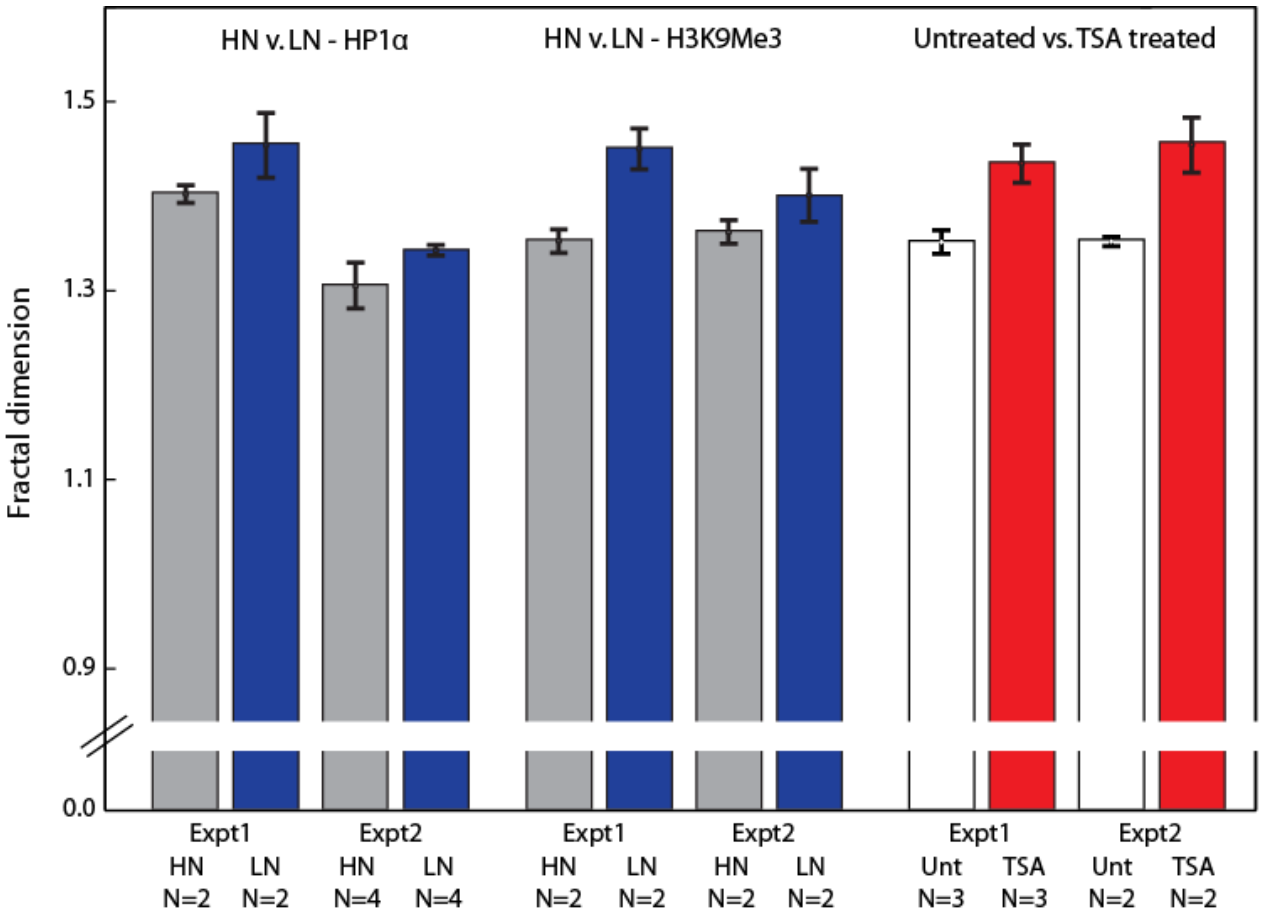

Fig. S10. Fractal dimension image analysis assessments are reproducible. Represented here are the statistics of each staining and subsequent analysis. For each replicate in each experiment, the mean of the fractal dimension of all cells was recorded, and the bars represent the means of those replicates, while the error bars are standard deviation. In the case of H3K27Me3 and TSA treatment experiments, the results were reproducible from one experiment to the next, while the overall numbers differ quite considerably from one experiment to the next in the HP1α experiment, although, importantly, the trend remains the same. Due to this discrepancy, the results reported in Fig. 3 of the manuscript represent the tallies from Expt. 2 only.

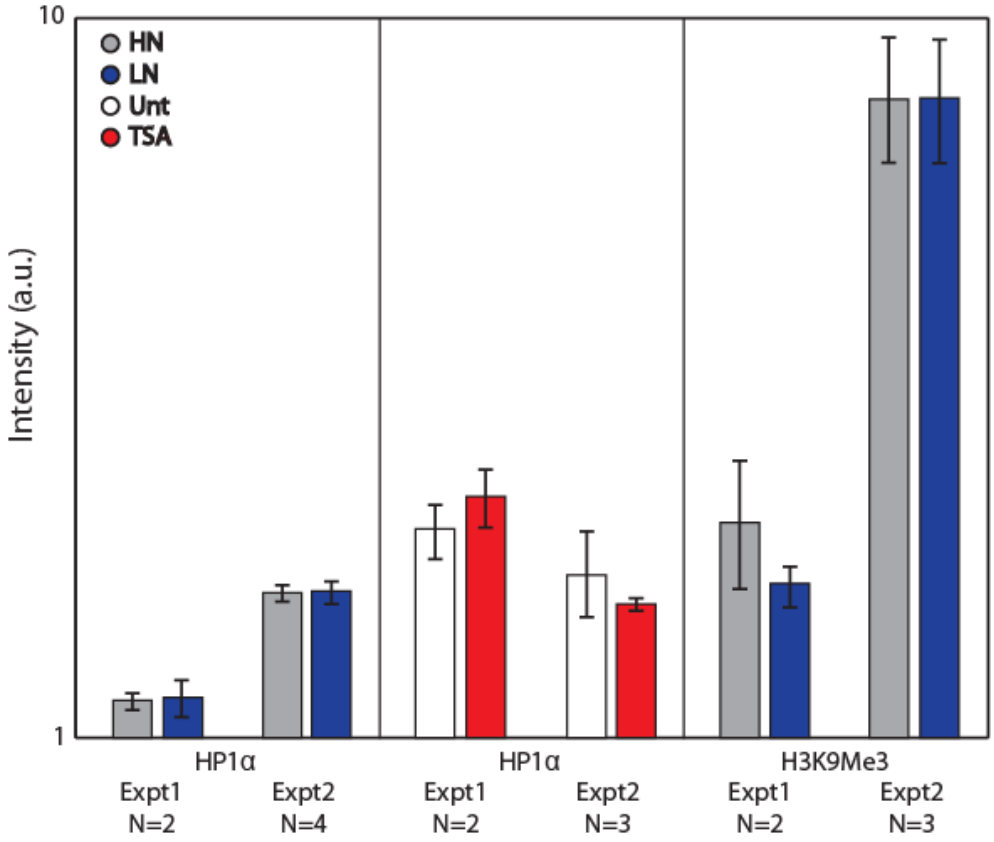

Fig. S11. Intensities of protein expression are reproducible and do not indicate differences between groups. Although the signal intensities are not reproducible from one experiment to the next, there is no trend to indicate that the overall protein expression is different in any case. There is a highly significant difference between H3K9Me3 expression in the first experiment of HN vs. LN, with a significantly lower expression in LN cells, but that difference disappears in the second experiment. In this figure, the data point indicates mean of the replicate average for each experiment and the error bars are the standard deviation of those means.